AIAA 2009-1027

47th AIAA Aerospace Sciences Meeting and Exhibit, 5-8 Jan 2009, Orlando, Florida

Correlated-k Distribution Method for Atomic Radiation in Hypersonic Nonequilibrium flows

Ankit Bansal*, M. F. Modest† and D. A. Levin‡
Department of Mechanical Engineering
Department of Aerospace Engineering
The Pennsylvania State University, University Park, PA 16802

I. Abstract

Radiation from the shock layer during atmospheric entry plays a significant role in the design of modern space vehicles, particularly in the design of the thermal protection system. This makes it necessary to predict the effects of radiation accurately and, at the same time, efficiently for the optimum design of new generation space vehicles. Line-by-line calculations are the most accurate method to solve the radiative transfer equation (RTE); however, they are not practical because of their large computational cost. In this work a correlated-*k* distribution method has been developed for the most important atomic species (N and O, as well as their ions), which provides great accuracy with high numerical efficiency for the evaluation of radiative transfer in a hot plasma. Challenges posed by typical nonequilibrium gas conditions in the plasma were overcome by splitting the full spectrum into a number of nonoverlapping part-spectra. Results for one-dimensional inhomogeneous gas slabs are presented and compared with line-by-line benchmarks and the full-spectrum correlated-*k* (FSCK) model, showing very good accuracy in typical nonequilibrium gas conditions as are found in atmospheric reentry of space vehicles.

Nomenclature

a	nongray stretching function of k-distributions, dimensionless
b	line width, Å
c	speed of light, 2.9979×10^8 ms^{-1}
f	k-distribution, cm
g, g'	cumulative k-distribution
h	Planck's constant, 6.6262×10^{-34} Js
I	intensity, (W/m^2 cm)
k	reordered absorption coefficient, cm^{-1}
m	atomic mass, kg
$N, \underline{N}$	number density (vector)
T	temperature, K
V	volume, m^3
Greek	
κ	absorption coefficient, cm^{-1}
λ	wavelength, Å

*Graduate student, Department of Mechanical Engineering; azb162@psu.edu
†Distinguished professor, Department of Mechanical Engineering; mfm@engr.psu.edu
‡Professor, Department of Aerospace Engineering; dalevin@psu.edu

$\underline{\phi}$ gas state vector

Subscripts

0 reference state
b blackbody
bf bound-free
cl line center
D Doppler
e electron
ff free-free
k at a given value of reordered absorption coefficient variable
g at a given value of cumulative *k*-distribution
P Planck-mean
S Stark
U upper state
L lower state
λ at a given wavelength

II. Introduction

The design of new generation space vehicles will require optimum design of thermal protection systems (TPS). Accurate computations of the radiative heating load are absolutely necessary for the design of TPS, because uncertainties of the order of even 20% may have important system design implications. However, modelling radiative sources in hypersonic shocklayers and fluxes onto space crafts is a highly complex task. Recently, a number of such studies have been made, primarily in the context of the Huygens and Stardust missions.[1] NEQAIR96[2] has been the most widely used code for performing such calculations. NEQAIR96 provides line-by-line data of nonequilibrium radiative properties of hypersonic shock layer plasmas, along with a primitive one-dimensional radiation transport algorithm.

The radiation transfer equation (RTE) is a five dimensional (3 space coordinates and 2 directions) integro-differential equation and is, consequently, very expensive to solve. To make nonequilibrium shocklayer radiation calculations possible, a number of simplifications had to be made. Most efforts, so far, have been directed toward solving the RTE with flow solvers in an uncoupled manner. However, the presence of a strong radiation field may significantly alter the population distribution of various radiating species, and a coupled radiative transport solution is desired for a more accurate solution. Absorption coefficients of high temperature air plasma, as found in the shock layer of space craft during atmospheric entry, have very erratic spectral behavior, varying by orders of magnitude over tiny spectral regions. The strong spectral structure of the radiative emission requires a line-by-line (LBL) solution of the RTE at several hundred thousand wavelengths, making it prohibitively expensive. Also, most of the simulations done to date have been limited to simplified quasi-one-dimensional geometries (simple line-of-sight or tangent slab calculations). These assumptions may lead to very unreliable predictions of radiative heat load onto the space craft. Due to the use of the LBL method, coupled solutions with NEQAIR, even for simple one-dimensional geometries, would be prohibitively expensive. More recently, Sohn *et al.*[3] have developed an efficient databasing scheme that has resulted in a significant reduction of the computation time for spectral coefficients vis-a-vis NEQAIR. This database uses the Quasi-Steady-State (QSS) assumption to model nonequilibrium electronic state populations for various energy states. Sohn *et al.* have demonstrated that their databasing scheme can be applied efficiently to generate spectral coefficients for a given flow condition. However, solving the RTE line-by-line remains computationally very expensive. It is, therefore, absolutely necessary to develop a spectral radiation model that can predict radiative heating loads in hypersonic shock layers accurately and, at the same time, efficiently.

It has been shown that, for a small spectral interval in a homogeneous medium, the absorption coefficients can be reordered into a monotonic *k*-distribution, which yields exact results at a fraction of the computational cost required by line-by-line methods.[4,5] More recently, such *k*-distribution methods have been applied to the full spectrum and to inhomogeneous media.[6,7] While the *k*-distribution method is exact for a homogeneous medium, significant errors may occur when applied to strongly inhomogeneous media. Over the years a number of new adaptations of *k*-distribution method have evolved. The problem of inhomogeneity is adressed by using one of the two different approaches: the scaling approximation or the assumption of a correlated *k*-distribution.[7] Both the scaled and correlated-*k* approaches

may result in significant errors when dealing with inhomogeneous media because neither the scaled nor the the correlated assumptions are ever truly accurate. The resulting errors and the applicability of scaled and correlated-*k* method have been discussed by Modest.[7] It was recognized[8–10] that, in high temperature combustion applications, with significant temperature changes totally different spectral lines dominate the radiative transfer, and the assumption of a correlated absorption coefficient breaks down. Similarly, in a mixture of gases the correlation breaks down in the presence of strong concentration gradients, as recognized by Modest and Zhang.[6] To overcome some of these difficulties, Modest and Zhang have developed the multi-scale full-spectrum correlated-*k* distribution method MSFSCK,[11] where different lines are placed into separate "scales" based on their temperature dependence, and the multi-group full-spectrum correlated-*k* distribution method MGFSCK,[12] where different spectral positions are placed into different spectral groups according to their temperature and pressure dependence. The multi-group model has the advantage that it avoids the problem of overlap between the spectral groups. In contrast, in the MSFSCK method the approximate treatment of overlap between different scales may lead to additional inaccuracy.

The use of the correlated-*k* method for solving high-temperature shock-generated radiation problems appears very attractive; however, applying it to hypersonic plasmas introduces a number of new difficulties due to thermodynamic nonequilibrium and the presence of a significant number of radiating species. The shock layer of a reentry space vehicle is marked by the presence of extreme temperature and concentration gradients. The nonequilibrium flow field cannot be represented by a single temperature, and the radiation field is governed by a number of collisional processes. Finally, monatomic species have relatively few spectral lines, but of extreme opacity, making the behavior of line wings of overriding importance. These phenomena make the shock radiation problem very challenging from an FSCK point of view. For the case of atomic radiation we can take advantage of both the multi-group approach and the multi-scale approach. There are only a few atomic lines that cover only a small part of the spectrum. Most of the atomic lines are very narrow and do not overlap with other lines. Atomic lines that do overlap have similar temperature and number density dependence. Thus, atomic lines can be sorted into a number of nonoverlapping spectral groups, with each group also forming a different scale.

In this work, we have developed and applied the correlated-*k* method to the solution of the radiation transfer problem of monoatomic species in a shock layer as found in hypersonic nonequilibrium flows. The flow in such case is highly dissociated and radiation from the atomic species makes far-and-away the most significant contribution. In the present first attempt we have developed the *k*-distribution method for the two important radiating species N and O and their ions. The model has been tested with the Stardust flow field. In future work, we will extend the method to include other atomic and diatomic species. The new model will be applied to several Earth and Mars atmospheric entry conditions. However, the model will be developed in such a way that it can be applied to any arbitrary entry conditions on other planetary bodies.

III. Atomic radiation

In high-temperature nonequilibrium flows diatomic species may become highly dissociated and emission from the two atomic species N and O, including bound-bound, bound-free and free-free transitions, can be the major source of radiation from the shock layer. For atomic radiation, atomic bound-bound lines contribute more to the total radiation than the bound-free and free-free transitions. Atomic lines result from transitions from one electronic state to the other. The details of the various electronic states of N and O, as used in NEQAIR and the database developed by Sohn *at al.*,[3] are given in Table 1.[13] The table lists the term-symbols of different energy states and values of energy and degeneracy for each of the states. The higher electronic states in this table are composite states formed by combining a number of different electronic states. Some electronic transitions are more probable than others and, therefore, some lines are stronger than others.

Most atomic lines are optically very thick and have strong self absorption characteristics. More than 90% of emission from these lines may be absorbed by the line itself over distances as short as 1mm. Thus, atomic line wings, rather than the line centers, are most important from a heat transfer point of view. Consequently, it is very important to represent the line shape accurately. Line shape can most realistically be described by the Voigt profile.[2,14] The Voigt profile is defined by Lorentzian and Gaussian line half-widths at half-height. The line width is an important parameter as it specifies how far from the line center a line retains its strength before its contribution becomes insignificant. Usually, with a Voigt line profile a strong atomic line may remain important up to 25 to 50 line half-widths on each side of the line, since it is optical thicknesses of order unity that contribute most to the radiative transfer. The Lorentzian

width depends on a number of broadening mechanisms. For the case of high-temperature plamas having high electron number densities, the Lorentz width is essentially governed by Stark broadening, while the Gaussian width comes from Doppler broadening. The Stark width b_S and Doppler width b_D can be written as[15]

$$b_S = 2b_{S,ref}\left(\frac{T_e}{T_{ref}}\right)^{0.33}\frac{N_e}{N_{e,ref}} \tag{1}$$

$$b_D = \lambda_{cl}\sqrt{\frac{2kT\ln 2}{mc^2}} \tag{2}$$

where $b_{S,ref}$ is a reference Stark width value at a reference electron temperature of $T_{ref} = 10,000$K, and reference electron density $N_{e,ref} = 10^{16}\text{cm}^{-3}$; λ_{cl} is the wavelength at the center of an atomic line and m is the mass of the radiating atom.

In this work we will use the database developed by Sohn *et al.* to calculate the absorption and emission coefficients for different flow conditions. N has about 170 bound-bound lines while O has about 86 lines.[2,3] At a resolution of 0.005 Å, it requires on an average 1000 spectral points to describe a single line spread over 25-50 line half-widths on each side. This makes the line-by-line RTE evaluations very expensive as a total of some quarter million RTE evaluations will be required.

IV. Formulation of full spectrum correlated-*k* method

To understand the various adaptations of FSK methods, it is essential to have a grasp of the basic formulation of the method. In *k*-distributions the erratic spectral absorption coefficient is reordered into a monotonically increasing function over a narrow band, part spectrum or full spectrum. All *k*-distribution methods to date have been developed for the case of thermodynamic equilibrium, where the radiation field is represented by a single temperature. When the state of a gas in not in thermodynamic equilibrium, it cannot be described by a single temperature. However, the formulation of the *k*-distribution method for the nonequilibrium case is quite similar with one major difference being the definition of the Planck function. For any given atomic bound-bound transition the population ratio of upper to lower electronic states, N_L/N_U, replaces the exponential term in the Planck function.[2] The radiative transfer equation (RTE) for an absorbing and emitting hypersonic plasma can then be written as[14]

$$\frac{dI_\lambda}{ds} = \kappa_\lambda[I^{ne}_{b\lambda} - I_\lambda] \tag{3}$$

where $I^{ne}_{b\lambda}$ is Planck function for the nonequilibrium case, and is defined as[2]

$$I^{ne}_{b\lambda} = \frac{2hc^2}{\lambda^5}\frac{N_U}{N_L - N_U} \tag{4}$$

Eq. (3) is reordered into a *k*-distribution by multiplying it with the Dirac-delta function $\delta(k - \kappa_\lambda(\lambda, \underline{\phi}_0))$, followed by integration over the entire spectrum. Here $\kappa_\lambda(\lambda, \underline{\phi}_0)$ is the absorption coefficient evaluated at some reference state $\underline{\phi}_0 = (T, T_e, \underline{N}_0)$, where $\underline{N}_0$ is the number density vector specifying concentrations of the species (neutral, ion and electron) at the reference state. This leads to

$$\frac{dI_k}{ds} = k^*(\underline{\phi}, k)[f(\underline{\phi}, \underline{\phi}_0, k)I^{ne}_b(\underline{\phi}) - I_k] \tag{5}$$

provided that at every wavelength across the entire spectrum, where $\kappa_\lambda(\lambda, \underline{\phi}_0) = k$, we must also have a unique value for $\kappa_\lambda(\lambda, \underline{\phi}) = k^*(\underline{\phi}, k)$ everywhere within the medium. In Eq. (5) I_k and f are defined as

$$I_k = \int_0^\infty I_\lambda \delta(k - \kappa_\lambda(\lambda, \underline{\phi}_0))d\lambda \tag{6}$$

$$f(\underline{\phi}, \underline{\phi}_0, k) = \frac{1}{I^{ne}_b}\int_0^\infty I^{ne}_{b\lambda}(\lambda, \underline{\phi})\delta(k - \kappa_\lambda(\lambda, \underline{\phi}_0))d\lambda \tag{7}$$

where f is the Planck function-weighted full spectrum k-distribution, which depends on reference state conditions $\underline{\phi}_0$ and local conditions $\underline{\phi}$. The total intensity I can be obtained by integrating I_k over the reordered k-space. The k-distribution can be considered as a probability density function (PDF), giving the probability that the absorption coefficient will attain a value k. The k-distribution f has very erratic behavior and integration in k-space is very inconvenient. However, Eq. (5) can be transformed into the much smoother g-space by dividing it by the k-distribution at the reference state $f(\underline{\phi}_0, \underline{\phi}_0, k)$, leading to

$$\frac{dI_g}{ds} = k^*(\underline{\phi}_0, \underline{\phi}, g)[a(\underline{\phi}, \underline{\phi}_0, g)I_b^{ne}(\underline{\phi}) - I_g] \tag{8}$$

with

$$I_g = I_k / f(\underline{\phi}_0, \underline{\phi}_0, k) = \int_0^\infty I_{b\lambda}^{ne}(\lambda, \underline{\phi})\delta(k - \kappa_\lambda(\lambda, \underline{\phi}_0))d\lambda \Big| f(\underline{\phi}_0, \underline{\phi}_0, k) \tag{9}$$

where, g is the cumulative k-distribution and $a(\underline{\phi}, \underline{\phi}_0, g)$ is a weight or nongray stretching function given by

$$g(\underline{\phi}_0, \underline{\phi}_0, k) = \int_0^k f(\underline{\phi}_0, \underline{\phi}_0, k)dk \tag{10}$$

$$a(\underline{\phi}, \underline{\phi}_0, g) = \frac{f(\underline{\phi}, \underline{\phi}_0, k)}{f(\underline{\phi}_0, \underline{\phi}_0, k)} = \frac{dg(\underline{\phi}, \underline{\phi}_0, k)}{dg(\underline{\phi}_0, \underline{\phi}_0, k)} \tag{11}$$

In numerical calculations it is difficult to evaluate the ratio of the k-distributions f, due to their erratic behavior (having singularities at each minimum and maximum of the absorption coefficient[7]); it is much more convenient to evaluate the derivative dg/dk, as indicated in Eq. (11).

Because atomic lines are spread over only a very small part of the spectrum, most of the k-distribution lies in the g-range $0.99 \le g \le 1$. Thus, for numerical precision reasons, it is preferable to redefine the cumulative k-distribution as

$$g'(\underline{\phi}, k) = 1 - g(\underline{\phi}, k) = \int_k^{k_{max}} f(\underline{\phi}_0, \underline{\phi}_0, k)dk \tag{12}$$

i.e., a monotonically *decreasing* function.

The formulation of the corelated-k method for atomic continuum radiation is exactly the same, again the only difference is in the definition of the Planck function, which for continuum radiation, can be defined in terms of emission and absorption coefficient as

$$I_{b\lambda}^{ne} = \frac{\varepsilon_{\lambda,bf} + \varepsilon_{\lambda,ff}}{\kappa_{\lambda,bf} + \kappa_{\lambda,ff}} \tag{13}$$

V. Reference state

In principle, the choice of reference state is irrelevant for a truly correlated k-distribution. However, since real k-distributions are not perfectly correlated, the choice of a proper reference state can have significant impact on overall solution accuracy. For the case of thermal equilibrium Modest and Zhang[6] have suggested a reference state based on volume-averaged mole fraction and Planck-mean temperature based on average emission from the volume. For the problem of nonequilibrium atomic radiation we adopt a similar approach to evaluate the reference state. The radiation process in a hot plasma is dominated by electron collisions. Therefore, the electron temperature is the most important parameter. The Planck function for the nonequilibrium case depends on electron temperature through electronic state population. The electron temperature for the reference state is taken as the Planck-mean temperature based on average emission from the volume. Translation temperature just affects Doppler broadening, and its value for the reference state $\underline{\phi}_0 = (T_0, T_{e0}, \underline{N}_0)$ is chosen as the volume average.

$$\underline{N}_0 = \frac{1}{V}\int_V \underline{N}dV \tag{14}$$

$$T_0 = \frac{1}{V}\int_V TdV \tag{15}$$

$$\kappa_P(\underline{\phi}_0) I_b^{ne}(\underline{\phi}_0) = \frac{1}{V} \int_V \kappa_P(\underline{\phi}) I_b^{ne}\left(\underline{\phi}\right) dV \tag{16}$$

where $\kappa_P(\underline{\phi})$ is the Planck-mean absorption coefficient and is given by

$$\kappa_P(\underline{\phi}) = \frac{1}{I_b(\underline{\phi})} \int_0^\infty \kappa_\lambda(\underline{\phi}) I_{b\lambda}^{ne}\left(\underline{\phi}\right) d\lambda \tag{17}$$

For all the different cases of nonequilibrium atomic radiation we considered, this reference state provides excellent accuracy. However, it is should be tested for many more flow conditions and radiation environments.

VI. Grouping Scheme for atomic lines

The *k*-distribution method is exact for a homogeneous medium and for truly correlated absorption coefficients. For the case of hypersonic nonequilibrium flow large temperature and concentration gradients are present within the shock layer, and for such a case atomic lines appear not to be well correlated. Absorption coefficients of atomic lines and the nonequilibrium Planck function as defined in Eq. (13) depend on the population of upper and lower electronic states. At higher temperatures upper states of the atom become more and more populated. Atomic lines resulting from transitions from any of these upper states become stronger in high temperature regions. The line strength strongly depends on electron temperature. The dependence of absorption line strengths on electron temperature for N and O are plotted in Fig. 1 for a few selected atomic lines. It can be observed from this figure that different atomic lines have distinct patterns of dependence on electron temperature. It can also be observed that lines plotted in the same color show similar behavior (red lines show a continuous gradual decay of line strength with electron temperature; blue lines continuously increase with temperature; green lines first decrease slightly, then strongly increase with temperature; and, finally, black lines first decrease with temperature before rising again gradually). All bound-bound lines of N and O have behavior similar to one or the other of these selected lines. This dependence is plotted for just one value of neutral, ion and electron populations. For different values of populations the dependence is quite similar. The distinct behavior of these atomic lines in different flow conditions results in uncorrelatedness between the *k*-distributions. Zhang and Modest[12] have shown that dividing the spectrum into different spectral groups, according to their absorption coefficient dependence on gas conditions, greatly improves the accuracy of the correlated-*k* method. We adopt a similar approach for the case of atomic lines. Transitions shown in the same color can be combined or put into the same group.

All 170 lines of N can be combined into three different nonoverlapping spectral groups, and similarly, all the 86 O lines can be combined into 4 different spectral groups. These spectral groups for N and O are shown in Figs. 2 and 3, respectively. As will be seen, it is also possible to combine similar groups of N and O, provided that separate groups do not overlap with each other. It can be observed from Fig. 1 that N and O groups, shown in the same color, can be combined together. Thus, we can reduce the total number of groups to four, each shown in a different color. Also, continuum radiation from both species is modelled as a separate group. Thus, the total spectrum for N and O mixtures can be divided into 5 groups.

The correlated-*k* method for the multi-group case can essentialy be developed in the same way as for the full spectrum.[12] If we divide the full spectrum into M different part-spectra, each containing one group, then for the m-th group, multiplying Eq. (3) by the Dirac-delta function $\delta(k_m - \kappa_\lambda(\lambda, \underline{\phi}_0))$, followed by integration across the m-th spectral group leads to

$$\frac{dI_{km}}{ds} = k(\underline{\phi}, k_m)[\, f_m(\underline{\phi}, \underline{\phi}_0, k_m) I_b^{ne}(\underline{\phi}) - I_{k_m}] \tag{18}$$

where

$$I_{km} = \int_{\lambda \in [\lambda_m]} I_\lambda \delta(k_m - \kappa_\lambda(\lambda, \underline{\phi}_0)) d\lambda \tag{19}$$

$$f_m(\underline{\phi}, \underline{\phi}_0, k_m) = \frac{1}{I_b^{ne}} \int_{\lambda \in [\lambda_m]} I_{b\lambda}^{ne}(\lambda, \underline{\phi}) \delta(k_m - \kappa_\lambda(\lambda, \underline{\phi}_0)) d\lambda \tag{20}$$

where f is the Planck function-weighted full spectrum k-distribution for the m-th group, which depends on reference state conditions $\underline{\phi}_0$ and local conditions $\underline{\phi}$. Similar to single group case, Eq. (18) can be transformed into the much smoother g-space, leading to

$$\frac{dI_{gm}}{ds} = k^*(\underline{\phi}_{0,m}, \underline{\phi}, g_m)[a_m(\underline{\phi}, \underline{\phi}_0, g_m)I_b^{ne}(\underline{\phi}) - I_{gm}] \tag{21}$$

with

$$I_{gm} = I_{km}/f_m(\underline{\phi}_0, \underline{\phi}_0, k_m) \tag{22}$$

$$g_m(\underline{\phi}_0, \underline{\phi}_0, k_m) = \int_0^{k_m} f_m(\underline{\phi}_0, \underline{\phi}_0, k_m)dk_m \tag{23}$$

$$a(\underline{\phi}, \underline{\phi}_0, g_m) = \frac{f_m(\underline{\phi}, \underline{\phi}_0, k_m)}{f_m(\underline{\phi}_0, \underline{\phi}_0, k_m)} = \frac{dg_m(\underline{\phi}, \underline{\phi}_0, k_m)}{dg_m(\underline{\phi}_0, \underline{\phi}_0, k_m)} \tag{24}$$

The total intensity I can be obtained by integrating I_{gm} over the reordered g-space and summing over all spectral groups, i.e.,

$$I = \sum_{m=1}^{M} \int_0^{g_{m,max}} I_{gm}dg_m \tag{25}$$

$$\sum_{m=1}^{M} g_{m,max} = 1 \tag{26}$$

VII. Sample calculations

To illustrate the validity of the correlated-k distribution method to model radiation transfer in hot plasmas containing the atomic species N and O, we will consider a few examples. The correlated-k method will be applied to one-dimensional problems, i.e., solving the RTE using the tangent slab approximation, and the results will be compared with those obtained from line-by-line calculations. Since k-distributions just reorder the absorption coefficient, the correlated-k method can be used together with any RTE solver. One-dimensional cases are investigated here for simplicity.

First, the correlated-k method will be applied to a simple two-cell problem. We take more severe inhomogeneous conditions of temperature and concentration than actually present in typical hypersonic shock layers. We will consider two cells, 1 cm thick each, bounded by cold black walls. An example for the conditions in the two cells is given in Table 2. These conditions have been appropriately chosen from actual shock layer conditions. Such two-cell problems with typical conditions serves as the acid test for the method because of its abrupt step-change in conditions. In actual applications gradients are much more benign and the accuracy of the correlated-k method can be expected to be better. In this example radiation from only bound-bound lines has been considered. Figure 4 shows the k-distributions for N and O for the conditions in Table 2. Here $\underline{\phi}_1$ represents the gas state in Cell 1 and $\underline{\phi}_2$ represents the gas state in cell 2. $k(\underline{\phi}_1, \underline{\phi}_2, g_1)$ is the k-distribution for the absorption coefficient at state $\underline{\phi}_2$ and Planck function at state $\underline{\phi}_1$. The effect of varying the Planck function on the k-distributions can be understood in terms of stretching of k in g space. In Fig. 4 this stretching is represented by lines AB and CD. For exactly correlated k-distributions the magnitude of stretching in g space would be the same for all flow conditions, and the lines ABCD should form a rectangle. It is clear from this figure that for such highly nonhomogeneous and nonequilibrium gas conditions k-distributions are correlated neither for N nor O.

In Table 3 the heat fluxes coming out of the cold cell are compared. We consider two cases: (i) a single group for each species, (ii) 3 groups for N and 4 groups for O. It is clear that there is significant improvement in the accuracy of the correlated-k method once atomic lines are grouped according to their absorption characteristics. For both N and O the error reduces to below 2% for the multi-group case. In the same table the heat flux results for the mixture of N and O are also compared. The total heat flux from the mixture is found to be almost exactly equal to the sum of the indvidual gas contributions, indicating that the effect of overlap between N and O lines is not significant. As discussed in Section VI, the similar groups of N and O are combined for a total of four groups for the mixture. The error in heat

flux for this case remains below 2%, indicating that the 4-group correlated-*k* method developed in this paper can be applied to gas mixtures of N and O.

In the second example the correlated-*k* method is applied to the solution of the RTE in actual flow conditions. As an example we will take the peak heating stagnation-line flow field of the Stardust reentry vehicle. Number densities and temperature values for this flow field are shown in Fig. 5. Again, we will consider the cases of single and multiple groups of lines. In Fig. 6 the local heat flux and its divergence (i.e., the radiative source in the energy equation) from an N and O mixture along the stagnation line are compared. Reasonable accuracy is obtained when a single group is used for the mixture, including bound-free and free-free components (i.e., the standard FSCK approach), with errors below 5% (compared to the wall flux) except in the unimportant free-stream region. Excellent agreement between the line-by-line and correlated-*k* results is achieved if the grouping scheme is used. There is 0.24% error in the radiative heat flux onto the space craft for the case of four groups, while the single group method has an error of 4.20%. The maximum error along the stagnation line is found to be 2% for the case of 4 groups, while the single group approach has a maximum error of 12% in the free stream.

In above examples the RTE was integrated in *g*-space using the trapezoidal rule with 250 integration points for each group, requiring 250 RTE evaluations (single group), to 1250 RTE evaluations (five groups), as opposed to more than 200,000 evaluations required by line-by-line calculations. Since *k*-distributions are very smooth, a more efficient integration scheme, such as Gaussian quadrature, can be employed to integrate the RTE solutions. The above two cell problem was also solved using a 16 point Gaussian quadrature scheme. The cold wall heat flux results from the two integration schemes are compared in Table 4. With Gaussian quadrature, the error remains below 2.5% both for N and O. Thus, the number of RTE evaluation can be reduced by using an efficient integration scheme, while maintaining very good accuracy. Because atomic lines tend to be very opaque, standard Gaussian quadrature is not ideal, since it assigns most quadrature points to large *k*-values. In future work we hope to reduce the number of integration points to 8-10 per group by further optimizing the quadrature scheme.

VIII. Conclusions

The correlated-*k* method was developed for atomic radiation from N and O species in a nonequilibrium flow field. Atomic lines were separated into groups according to their absorption characteristics and electronic transitions. The agreement between line-by-line and correlated-*k* results is excellent if atomic lines are sorted into a small number of groups. The *k*-distribution method is vastly more efficient than the line-by-line method. In the line-by-line method approximately one quarter million evaluations of RTE must be performed, while in the correlated-*k* method we used 250 RTE evaluations for each group, with a total of 1000 evaluations for 4 groups. Using more efficient integration schemes, like Gaussian quadrature, further reduces the total number of evaluations. In future work we will also prepare a database of standard *k*-distributions, from which *k*-distributions for arbitrary flow conditions can be calculated through look-up and interpolation, thus futher increasing the efficiency of the *k*-distribution method.

i	n	E,cm^{-1}	g	States included
N atom, E_∞ = 117,345 cm^{-1}				
1	2	0	4	$2p^3\ ^4S$
2	2	19228	10	$2p^3\ ^2D$
3	2	28840	6	$2p^3\ ^2P$
4	3	83337	12	$3s\ ^4P$
5	3	86193	6	$3s\ ^2P$
6	3	95276	36	$3p\ ^4D$, $3p\ ^4P$, $3p\ ^4S$
7	3	96793	18	$3p\ ^2S$, $3p\ ^2D$, $3p\ ^2P$
8	4	103862	18	$4s\ ^4P$, $4s\ ^2P$
9	3	104857	60	$3d\ ^4F$, $3d\ ^4P$, $3d\ ^4D$
10	3	104902	30	$3d\ ^2P$, $3d\ ^2F$, $3d\ ^2D$
11	4	107082	54	$4p\ ^2S$, $4p\ ^4D$, $4p\ ^4P$, $4p\ ^2D$, $4p\ ^4S$, $4p\ ^2P$
12	5	110021	18	$5s\ ^4P$, $5s\ ^2P$
13	4	110315	90	$4d\ ^2P$, $4d\ ^4F$, $4d\ ^4D$, $4d\ ^2F$, $4d\ ^4P$, $4d\ ^2D$
14	4	110486	126	$4f\ ^4D$, $4f\ ^4F$, $4f\ ^4G$, $4f\ ^2D$, $4f\ ^2F$, $4f\ ^2G$
15	5	111363	54	$5p\ ^4S$, $5p\ ^4P$, $5p\ ^4D$, $5p\ ^2S$, $5p\ ^2P$, $5p\ ^2D$
16	5	112851	90	$5d\ ^2P$, $5d\ ^4F$, $5d\ ^4D$, $5d\ ^2F$, $5d\ ^4P$, $5d\ ^2D$
17	5	112929	288	$5f\ ^4D$, $5f\ ^4F$, $5f\ ^4G$, $5f\ ^2D$, $5f\ ^2F$, $5f\ ^2G$, $5g\ ^4F$
18	6	114298	648	$n = 6$
19	7	115107	882	$n = 7$
20	8	115631	1152	$n = 8$
21	9	115991	1458	$n = 9$
22	10	116248	1800	$n = 10$
O atom, E_∞ = 109,837 cm^{-1}				
1	2	78	9	$2p^4\ ^3P$
2	2	15868	5	$2p^4\ ^1D$
3	2	33792	1	$2p^4\ ^1S$
4	3	73768	5	$3s\ ^5S$
5	3	76795	3	$3s\ ^3S$
6	3	86629	15	$3p\ ^5P$
7	3	88631	9	$3p\ ^3P$
8	4	95757	8	$4s\ ^5S$, $4s\ ^3S$
9	3	97445	40	$3d\ ^5D$, $3d\ ^3D$
10	4	99313	24	$4p\ ^5P$, $4p\ ^3P$
11	5	102227	8	$5s\ ^5S$, $5s\ ^3S$
12	4	102881	96	$4d\ ^5D$, $4f\ ^5F$, $4d\ ^3D$, $4f\ ^3F$
13	5	103869	24	$5p\ ^5P$, $5p^3P$
14	5	105394	168	$5d\ ^5D$, $5f\ ^5F$, $5g\ ^5G$, $5d\ ^3D$, $5f\ ^3F$, $5g\ ^3F$
15	6	106639	288	$n = 6$
16	7	107583	392	$n = 7$
17	8	108117	512	$n = 8$
18	9	108478	648	$n = 9$
19	10	108734	800	$n = 10$

Table 1. Details of electronic states[13] of N and O

	Cell 1	Cell 2
T, K	24343.6	15011.3
T_e, K	19009.8	8578.3
N, /cm^3	2.05×10^{16}	3.41×10^{16}
N^+, /cm^3	1.36×10^{15}	2.71×10^{15}
O, /cm^3	6.75×10^{15}	1.12×10^{16}
O^+, /cm^3	8.91×10^{13}	2.12×10^{11}
N_e, /cm^3	2.09×10^{15}	3.10×10^{15}

Table 2. Flow conditions for the two cells

	line by line		correlated-*k*	error
N	204.02	1 group	216.68	6.21%
		3 groups	200.25	1.85%
O	15.61	1 group	16.47	5.56%
		4 groups	15.71	0.63%
N + O	219.87	1 group	235.61	7.16%
		7 groups	215.96	1.77%
		4 groups	215.51	1.98%

Table 3. Heat flux exiting the cold cell(W/cm^2)

	250 *g* points		16 points Gauss quadrature	error
N	200.25	3 groups	204.47	2.11%
O	15.71	4 groups	15.38	2.07%
N + O	215.51	4 groups	220.91	2.48%

Table 4. Heat flux exiting the cold cell(W/cm^2)

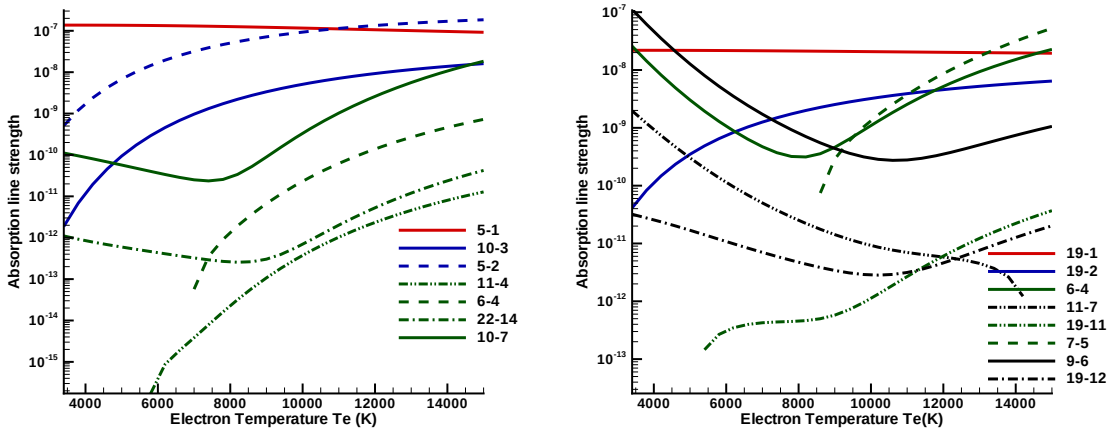

Figure 1. Dependence of absorption line strength on electron temperature N (left) and O (right)

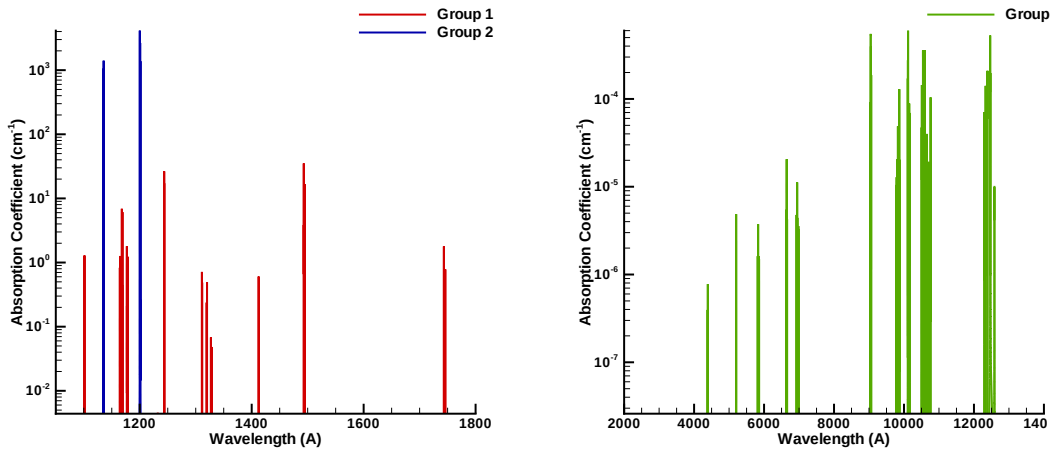

Figure 2. Spectral groups of atomic lines for N

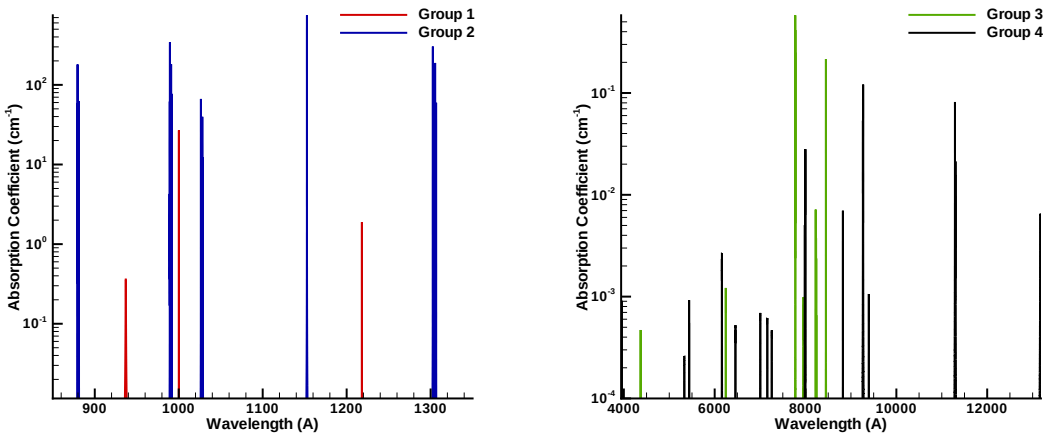

Figure 3. Spectral groups of atomic lines for O

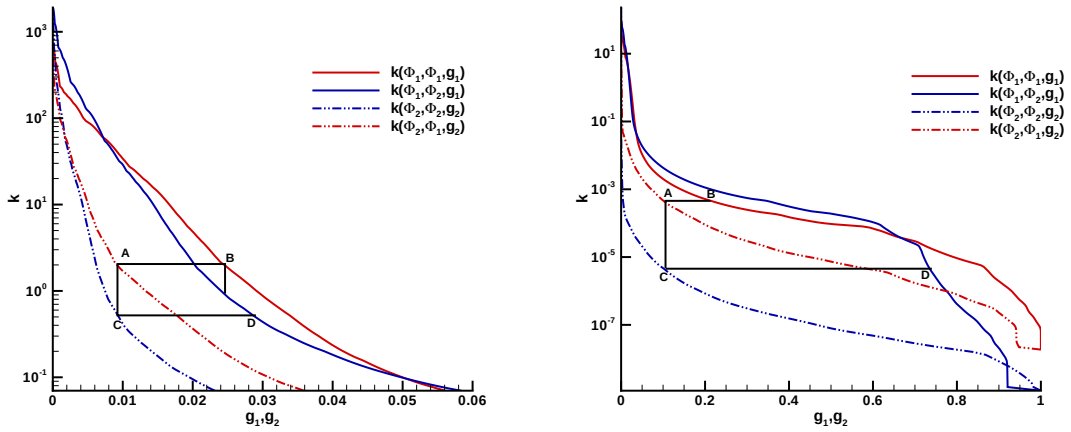

Figure 4. Comparison of k-distributions of N (left) and O (right)

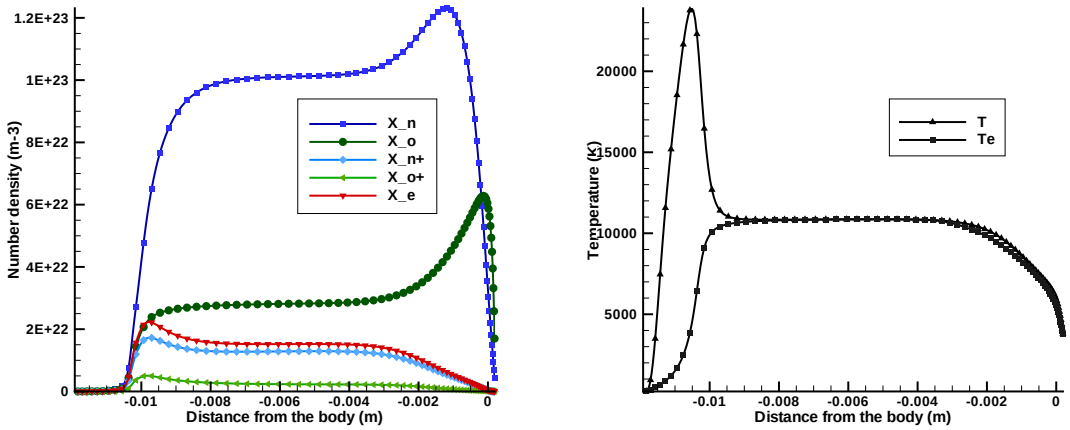

Figure 5. Stardust stagnation line flow field at peak heating

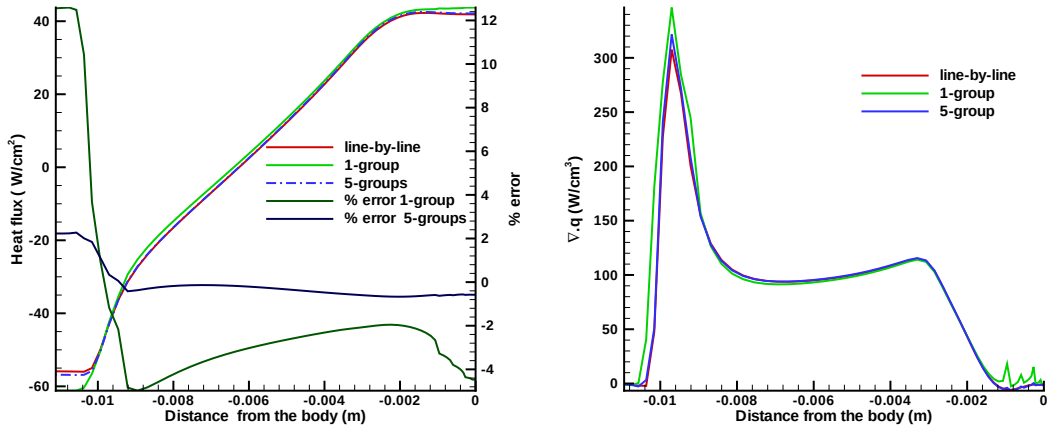

Figure 6. Comparison of heat flux and its divergence along stagnation line

References

[1]Liu, Y., Prabhu, D., Trumble, K. A., Saunders, D., and Jenniskens, P., "Radiation modelling for rhe reentry of the Stardust sample return capsule," *AIAA Paper No. 2008-1213*, 2008, 46th AIAA Aerospace Sciences Meeting and Exhibit Reno Navada.

[2]Whiting, E., Park, C., Liu, Y., Arnold, J., and Paterson, J., *NEQAIR96, Nonequilibrium and Equilibrium Radiative Transport and Spectra Program: User's Manual*, NASA/Ames Research Center, Moffett Field, CA 94035-1000, December 1996, NASA Reference Publication 1389.

[3]Sohn, I., Bansal, A., Modest, M. F., and Levin, D. A., "Advanced Radiation Calculations of Hypersonic Reentry Flows Using Efficient Databasing Schemes," *AIAA Paper No. 2008-4019*, 2008, 40th AIAA Thermophysics Conference, Seattle, Washington.

[4]Lacis, A. A. and Oinas, V., "A Description of the Correlated-*k* Distribution Method for Modeling Nongray Gaseous Absorption, Thermal Emission, and Multiple Scattering in Vertically Inhomogeneous Atmospheres," *Journal of Geophysical Research*, Vol. 96, No. D5, 1991, pp. 9027–9063.

[5]Goody, R. M. and Yung, Y. L., *Atmospheric Radiation – Theoretical Basis*, Oxford University Press, New York, 2nd ed., 1989.

[6]Modest, M. F. and Zhang, H., "The Full-Spectrum Correlated-*k* Distribution For Thermal Radiation from Molecular Gas–Particulate Mixtures," *Journal of Heat Transfer*, Vol. 124, No. 1, 2002, pp. 30–38.

[7]Modest, M. F., "Narrow-band and full-spectrum *k*-distributions for radiative heat transfer—correlated-*k* vs. scaling approximation," *Journal of Quantitative Spectroscopy and Radiative Transfer*, Vol. 76, No. 1, 2003, pp. 69–83.

[8]Rivière, P., Soufiani, A., and Taine, J., "Correlated-*k* and Fictitious Gas Methods for H_2O near 2.7 μm," *Journal of Quantitative Spectroscopy and Radiative Transfer*, Vol. 48, 1992, pp. 187–203.

[9]Rivière, P., Soufiani, A., and Taine, J., "Correlated-*k* and Fictitious Gas Model for H_2O Infrared Radiation in the Voigt Regime," *Journal of Quantitative Spectroscopy and Radiative Transfer*, Vol. 53, 1995, pp. 335–346.

[10]Rivière, P., Scutaru, D., Soufiani, A., and Taine, J., "A New $c - k$ Data Base Suitable from 300 to 2500 K for Spectrally Correlated Radiative Transfer in CO_2–H_2O Transparent Gas Mixtures," *Tenth International Heat Transfer Conference*, Taylor & Francis, 1994, pp. 129–134.

[11]Zhang, H. and Modest, M. F., "A Multi-Scale Full-Spectrum Correlated-*k* Distribution For Radiative Heat Transfer in Inhomogeneous Gas Mixtures," *Journal of Quantitative Spectroscopy and Radiative Transfer*, Vol. 73, No. 2–5, 2002, pp. 349–360.

[12]Zhang, H. and Modest, M. F., "Scalable Multi-Group Full-Spectrum Correlated-*k* Distributions For Radiative Heat Transfer," *Journal of Heat Transfer*, Vol. 125, No. 3, 2003, pp. 454–461.

[13]Park, C., *Nonequilibrium Hypersonic Aerothermodynamics*, Wiley, New York, 1990.

[14]Modest, M. F., *Radiative Heat Transfer*, Academic Press, New York, 2nd ed., 2003.

[15]Hartung-Chambers, L., "Predicting Radiative Heat Transfer in Thermochemical Nonequilibrium Flow Fields," *NASA Technical Memorandum 4564*, 1994.